Ionics (2018) 24:723–734
DOI 10.1007/s11581-017-2250-3

ORIGINAL PAPER

LiPON as a protective layer on graphite anode to extend the storage life of Li-ion battery at elevated temperature

Yong Liu[1] · Kai Xie[1] · Yi Pan[1] · Yujie Li[1] · Hui Wang[1] · Wei Lu[2] · Chunman Zheng[1]

Received: 5 June 2017 / Revised: 31 July 2017 / Accepted: 8 August 2017 / Published online: 25 August 2017

Abstract A thin-film lithium phosphorous oxynitride (LiPON) layer on the top of a graphite anode is synthesized via radio frequency magnetron sputtering, whereas the thickness of the film is about 0.3 ~ 1.3 μm. The field emission scanning electron microscopy on the samples confirms the even-coated layer on the anode, while the thickness of layer is reconfirmed by weighing the area density of sputtered anode. The storage experiment at elevated temperature of $LiNi_{0.8}Co_{0.15}Al_{0.05}O_2$/graphite cells with and without a LiPON layer on anode reveals that the LiPON layer on the anode would restrain the capacity loss when compared with bare anode. Moreover, it is found that a thicker LiPON layer on anode would provide better capacity retention during storage aging. Meanwhile, the electrochemical impedance spectroscopy is recorded during aging and its equivalent circuit simulation is proposed. Also, the anode surface morphology with and without a LiPON layer is observed before and after aging. Based on these investigations and analysis, we conclude that the LiPON layer on the top of the anode would act as a protective layer and improve the capacity retention during storage aging at elevated temperature.

Keywords LiPON layer · Graphite anode · Li-ion batteries · Storage life

✉ Yong Liu
liuzi244@sina.com

✉ Chunman Zheng
zhengchunman@hotmail.com

[1] College of Aerospace Science and Engineering, National University of Defense Technology, Changsha 410073, China

[2] Institution of Applied Physics, Army Officer Academy of PLA, Hefei 230031, China

Introduction

Recently, commercial lithium-ion batteries (LIBs) have performed well for most home electronic applications like cell phones and laptops. However, currently available LIB technology does not satisfy some of the performance goals for future hybrid electric vehicles (HEV) or plug-in hybrid electric vehicles (PHEV). One of the significant problems with current LIBs is their restrained lifetime, especially at elevated temperature while the aging progress would be accelerated [1]. In most automotive applications, the lifetime of LIBs is expected to be longer than 10 years [2].

The storage life is one of the key lifetime performances for LIB applications. Hence, many efforts have been made to investigate the aging mechanism and improve the storage life of commercial LIBs. Since LIBs are complex systems and the processes of their aging are even more complicated in application while the storage aging and cycle aging always occur in combination, the capacity decrease and power fading during aging do not originate from one single cause, but from a number of various processes and their interactions [3–8]; much more work is still needed for longer-life LIBs. However, the degradation reactions of electrolyte with lithium in anode, which leads the anode solid electrolyte interphase (SEI) sustaining growth on the graphite anode, are thought to be one of the main causes of the capacity loss during storage aging [9–12]. The anode SEI, formed in the cells' first few cycles and grown during aging, would act as the protective layer that inhibited the further decomposition of electrolyte on anode [13]. Therefore, a more stable and better formed SEI on anode would sustain the aging of LIBs [13–15].

A protective layer acted as an artificial SEI is an efficient way to acquire more stable SEI on anode [16–19]. The radio frequency (rf) magnetron sputtering is a direct way to synthesize a uniform layer on the basement material while lithium

phosphorous oxynitride (LiPON) could be chosen as the protective layer component, since LiPON is stable with Li and electrolyte in a wide potential window of 0–5.5 V and provides an acceptable ionic conductivity at room temperature of about 10^{-5}–10^{-6} S cm^{-1} [20, 21]. Meanwhile, LiPON has been reported as an efficient artificial SEI on Li and Si anode for better cycle performance [22–25].

However, sputtering LiPON layer on graphite anode would only isolate the top of the graphite anode from corrosion by the electrolyte during storage aging as the electrolyte would infiltrate into the inner gap of the graphite particle. To our best knowledge, we cannot know whether the top or the inner part of graphite anode plays a more important role in the capacity loss and SEI growing during storage aging, since the top of graphite anode has a shorter ionic transportation distance while the inner part has a bigger ionic transportation area when anode is corroded by electrolyte during storage aging.

In this work, different thicknesses of LiPON layer on anode are prepared and the storage life performance of Li-ion battery with and without LiPON layer on anode at elevated temperature is investigated. The cell electrochemistry impedance spectroscopy (EIS) during storage aging is recorded, and its equivalent circuit is simulated as it provides a deeper insight in the electrochemical process in the electrode/electrolyte interphase. Meanwhile, the anode surface morphology before and after aging is observed via SEM to analyze the surface stability with and without LiPON layer on anode.

Experiment

Cell design

Polymer-coated aluminum vacuum-sealed bag cells with a capacity of 200 ± 10 mAh were assembled with $LiNi_{0.8}Co_{0.15}Al_{0.05}O_2$ cathode and graphite anode with or without LiPON coating. Table 1 lists the components of the electrodes and electrolyte used and their specifications. Only one side of the collector was coated with active material to simplify the sputtering of LiPON. Electrodes were rolled before sputtering. Before the addition of electrolyte, the assembled cells were dried at 70 °C under vacuum for 24 h to remove any trace water. Electrolyte was added, and cells were sealed in argon-filled glove box under inert atmosphere with H_2O < 10 ppm and O_2 < 20 ppm. Sealed cells were laid in bake oven for 24 h at 45 °C to confirm the electrodes and separator were fully immersed with electrolyte. Then, cells were vacuum-sealed for electrochemistry test. At the same time, half cells (2016-type coin cell) with graphite as positive electrode (diameter of 15 mm) and Li foil as negative electrode were assembled with the same procedure of full cell as discussed before.

Table 1 Cell design description

Anode with Cu collector	
Graphite	93%
Carbon black	2%
LA133 binder	5%
Anode area density (without collector)	≈ 55 g/m^2
Electrode shape	5.5 cm × 22 cm
Cathode with Al collector	
$LiNi_{0.8}Co_{0.15}Al_{0.05}O_2$	93%
Carbon black	2%
PVDF binder	5%
Cathode area density (without collector)	≈ 110 g/m^2
Electrode shape	5.5 cm × 20 cm
Base electrolyte	1.2 M $LiPF_6$ EC: EMC 3:7 (vol%)
Separator	Cellgard 2320

The components of the electrodes and electrolyte used and their specifications

LiPON layer on anode preparation

The LiPON sputtering experiment was carried out by the rf magnetron sputtering equipment, using Li_3PO_4 as target and bare anode as substrate. In this work, the thickness of the LiPON layer was controlled by adjusting the sputtering time to keep the component uniformity of the LiPON layer. Anodes with three different sputtering time (5; 10; 15 min) samples were prepared, named sample 1, sample 2, and sample 3, respectively.

Electrochemistry test and storage life experiment

Half cells were cycled as the rate of C/10 (0.18 mA cm^{-2}) for five times at room temperature between 0.025 and 1.5 V. Before calendar life experiment, full cells were cycled for five times at room temperature to get fully activated after assembled. For storage aging experiment, cells were stored at open circuit in bake oven at 55 °C after being charged to 4.1 V. Three samples were taken out and cycled for about ten times after storage for every 30 days to monitor the stable capacity retention during aging. The EIS was recorded at open circuit during storage aging for every 15 days, measured at room temperature after cooled. The entire charge-discharge tests were under C/5 (40 mA) at room temperature between 2.75 and 4.1 V.

The intermediate EIS measurement of cells during aging was carried out in a frequency range between 100 kHz and 0.01 Hz with the 10 mV amplitude at room temperature, performed in Metrohm Autolab system. The equivalent circuit simulation of EIS was carried out by the program Zview.

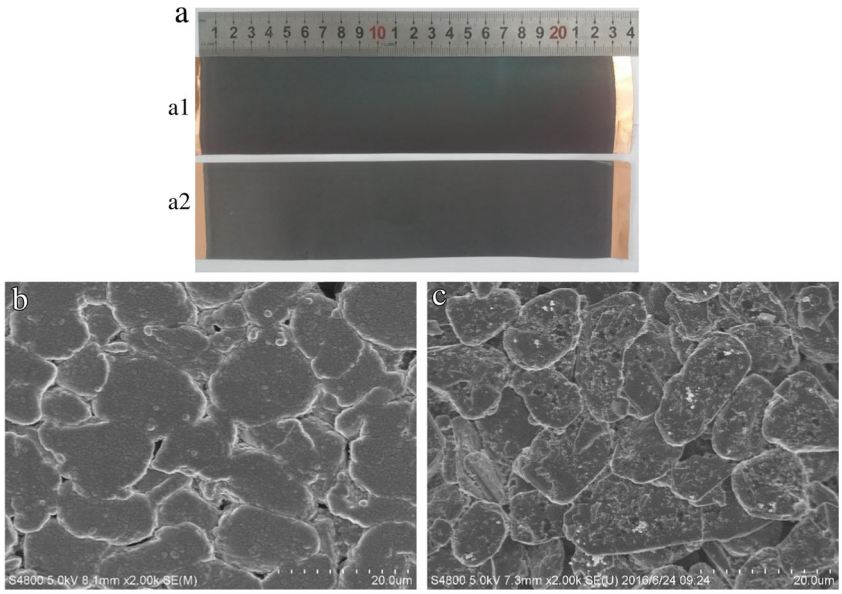

Fig. 1 The macro (**a**) and micro (**b**, **c**) graph comparison of anode with (a_1, **b**) and without (a_2, **c**) LiPON layer

Surface characterization

The surface morphology of anode was characterized before fabrication and again before and after aging by field emission scanning electron microscopy (SEM). The thickness of LiPON layer was estimated by SEM, along with weighing the area density of the sputtered anode. For SEM observation, cells were disassembled in Ar-filled glove box and slices of anode were extracted. The slice of anode was purified by DMC for three times and dried in vacuum for 12 h. During transformation of samples to SEM vacuum chamber, samples were exposed to air for about 30 s unfortunately. The SEM surface morphology of anode was investigated by Hitachi S-4800. For area density characterization, the weight before and after sputtering was recorded;

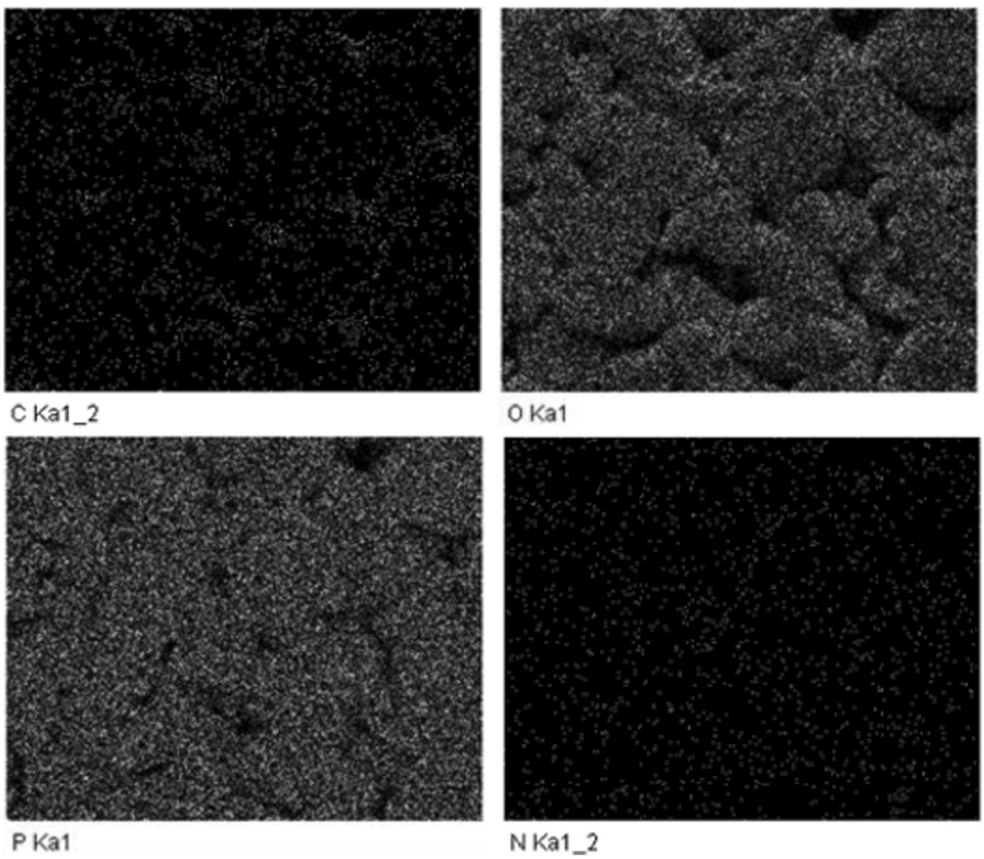

Fig. 2 The EDS elemental distribution of anode with LiPON layer (analysis of Fig. 1b)

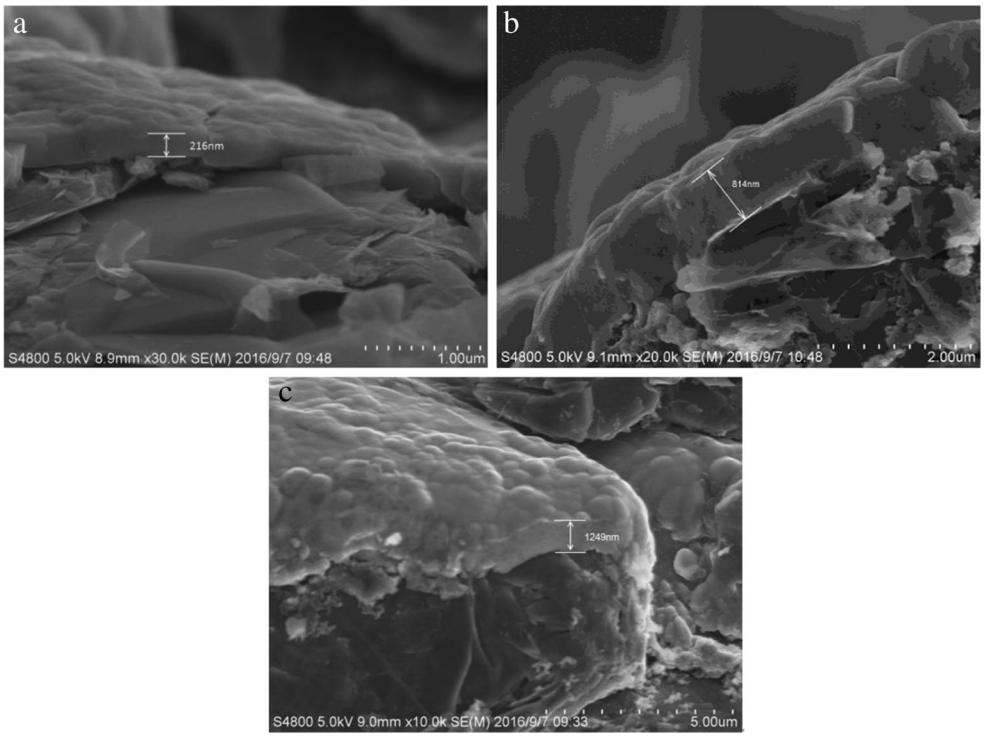

Fig. 3 SEM micrograph of sample 1 (**a**), sample 2 (**b**), and sample 3 (**c**) graphite anode

the area density was calculated by the equation $\rho = m/S$, where m represented the mass increased after sputtering; S represented the area of the sputtering zone.

Results and discussion

The characterization of LiPON layers

The morphology of the LiPON layer was characterized by SEM, compared with the bare anode. Part of the graph and SEM micrograph of anodes was showed in Fig. 1. As Fig. 1a–c shows, the anode with LiPON layer exhibits different surface features through macro and micro observation, compared with bare anode: The anode with the LiPON layer was much more shinning than the bare anode because of the glass state of the LiPON layer; Meanwhile, the gap between graphite particles was blocked or narrowed by the LiPON layer during the sputtering process as we could see from the top view of the anode (Fig. 1b and c). Also, the top view of SEM micrograph (Fig. 1b) on anode showed the LiPON layer on the graphite was not flat but with rough surface. The EDS analysis of Fig. 1b (anode with LiPON layer) as Fig. 2 depicts showed that the LiPON layer was uniformly sputtered on the graphite anode as the oxygen (O) and phosphorus (P) were uniformly distributed. Meanwhile, since the element carbon (C) was at low content, we could conclude that the top of the anode was fully covered by the LiPON layer.

The thickness of the LiPON layer was measured on the side view of the anode. As Fig. 3 shows, the estimated thicknesses were about 220, 810, and 1250 nm, respectively, for sputtering 5, 10, and 15 min. Meanwhile, the area density of LiPON on anode was measured to get the precise amount of LiPON layer on anode. The relationship of area density and thickness versus sputtering time was showed in Fig. 4. As can be seen from Fig. 4, the area density and the thickness exhibit a linear relationship of the same gradient with sputtering time. The linear relationship did not pass through the origin since it took time to activate enough Li_3PO_4 before the first LiPON emerged on the substrate. The estimated density of LiPON was about 2.6 ~ 3.0 g cm^{-3}, which was higher than the reported LiPON density [26] as the area used here was macro area, smaller than the real micro area.

To investigate the ionic conductivity of LiPON, a 2500-nm-thick LiPON was deposited between two metal electrodes,

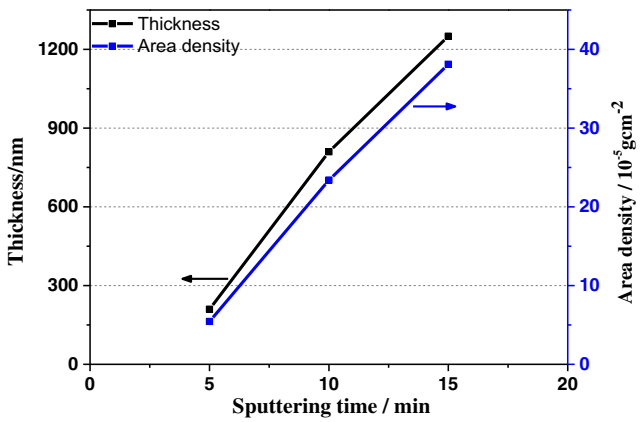

Fig. 4 Area density (blue) and estimated thickness (black) versus sputtering time

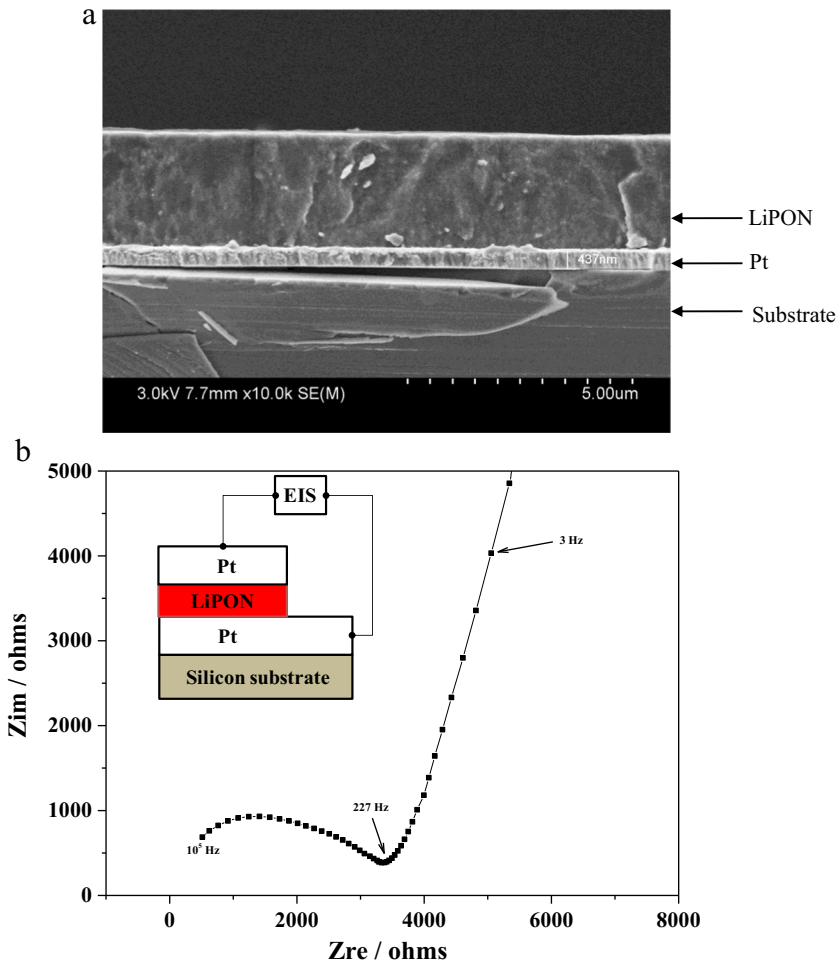

Fig. 5 SEM image of EIS test LiPON layer (**a**) and impedance data of the 2500 nm LiPON layer and corresponding sample setup (**b**)

as Fig. 5 shows. The EIS was measured at 25 °C. The specific ionic conductivity could be calculated via:

$$\sigma = \frac{d}{R \times S}$$

while d represented the thickness of the layer, S represented the specific electrode area of the test layer; R represented the resistance, determined by low frequency intersection with the real axis in the EIS spectrum. With this measurement, a conductivity of $5 \sim 10 \times 10^{-6}$ S cm^{-1} at 25 °C was estimated.

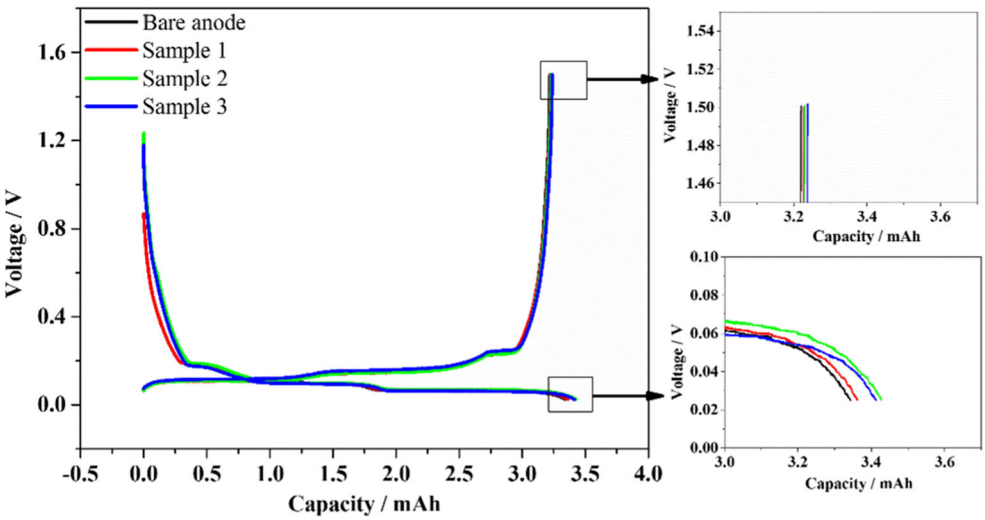

Fig. 6 The first lithiation and delithiation curves of the graphite/Li coin cell at C/10 (0.181 mA cm^{-2})

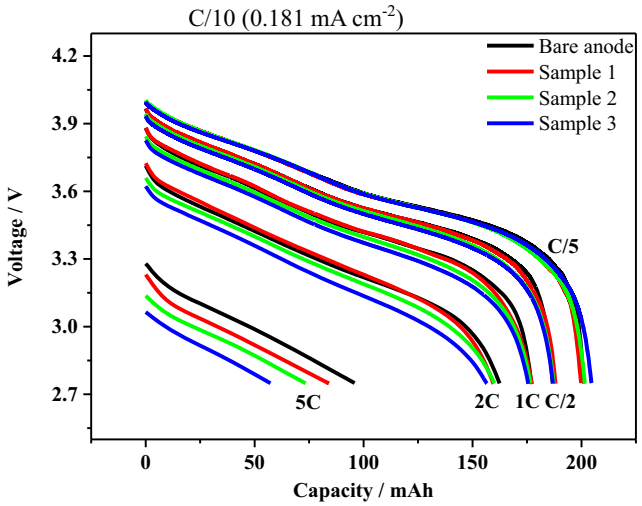

Fig. 7 The rate performances of the $LiNi_{0.8}Co_{0.15}Al_{0.05}O_2$/graphite full cell with and without LiPON layer on anode

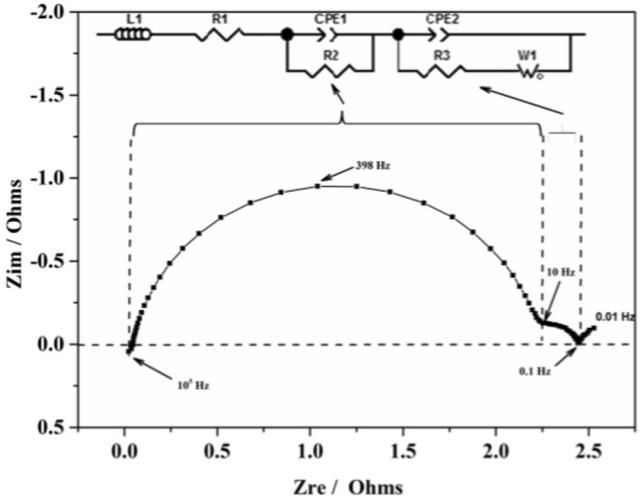

Fig. 9 A typical Nyquist plot of the test cell and the used equivalent circuit in this work

Cell performances

Figure 6 showed the first lithiation and delithiation curves of the graphite/Li coin cell at C/10 (0.181 mA cm^{-2}) with and without the LiPON layer on graphite electrodes. As seen in Fig. 6, the LiPON layer on graphite electrodes did not affect the graphite charge-discharge platform. But as showed in the magnified images, the first lithiation and delithiation capacities were improved with the addition of the LiPON layer, though the improvement was very weak. That indicated that the LiPON layer was

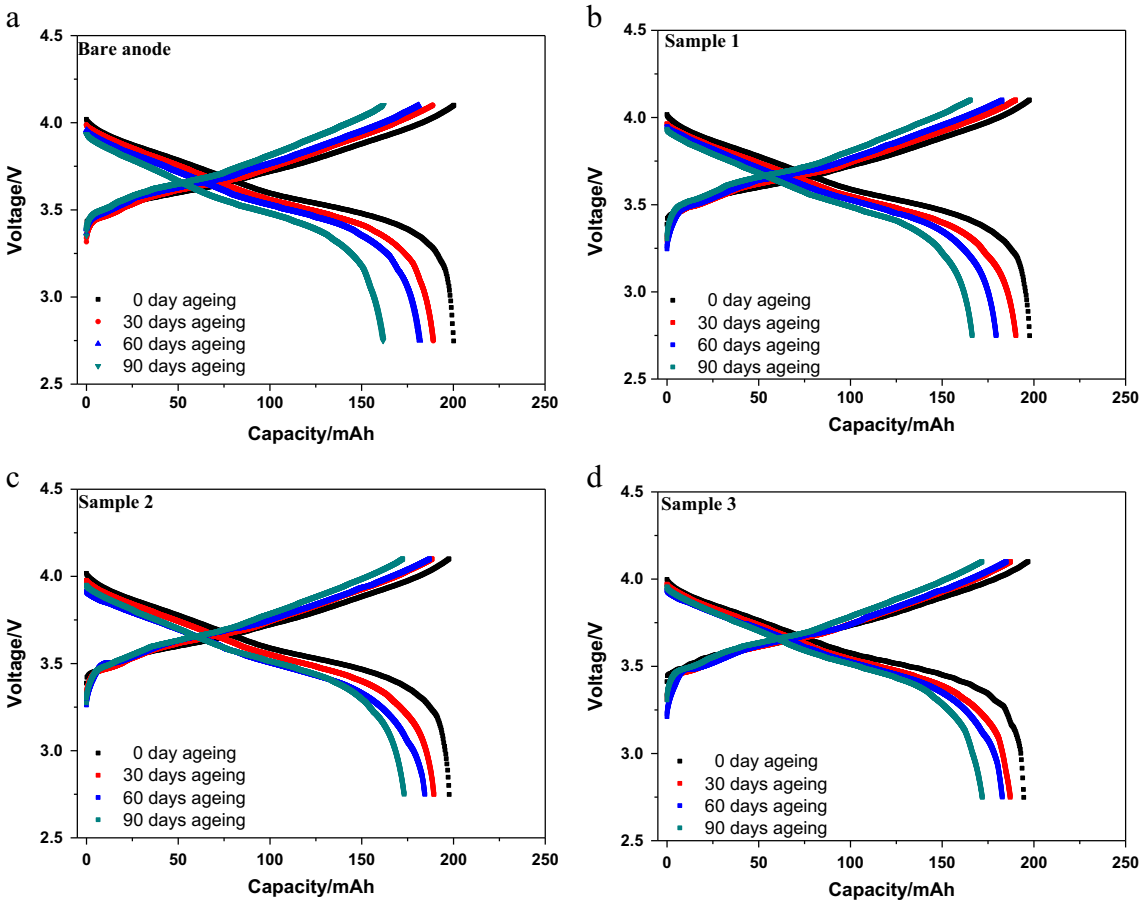

Fig. 8 The charge-discharge curves of cell with bare anode (**a**); sample 1 anode (**b**); sample 2 anode (**c**); sample 3 anode (**d**) after storage aged for every 30 days at 55 °C

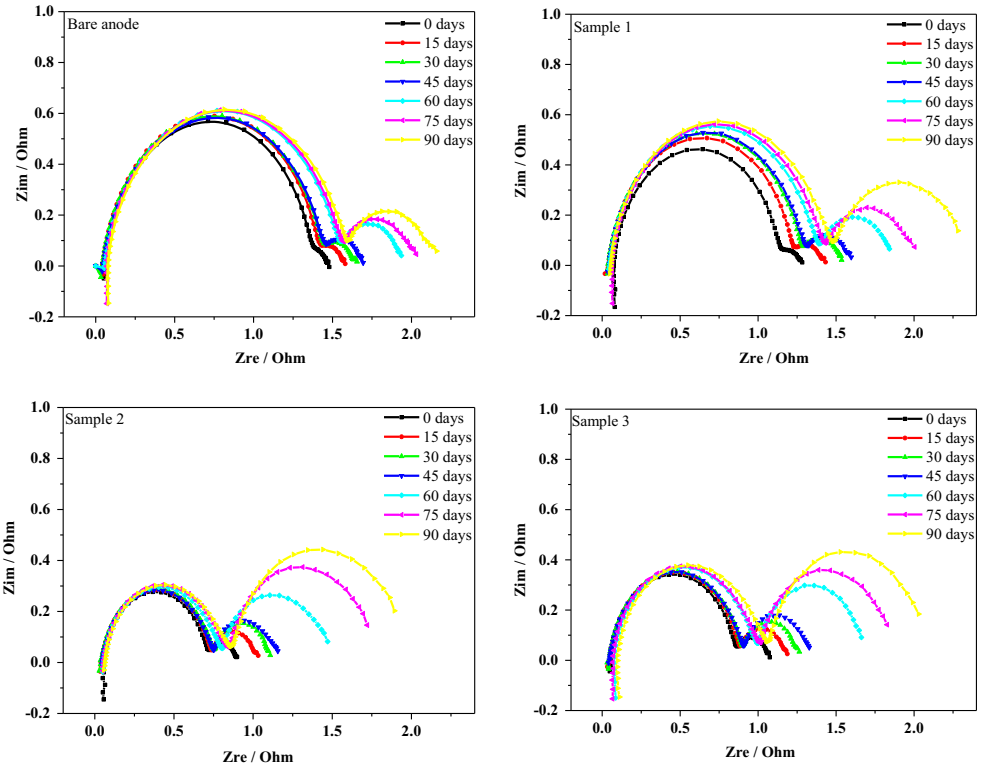

Fig. 10 The Nyquist plot of cells with and without LiPON layer on anode during storage aging at 55 °C

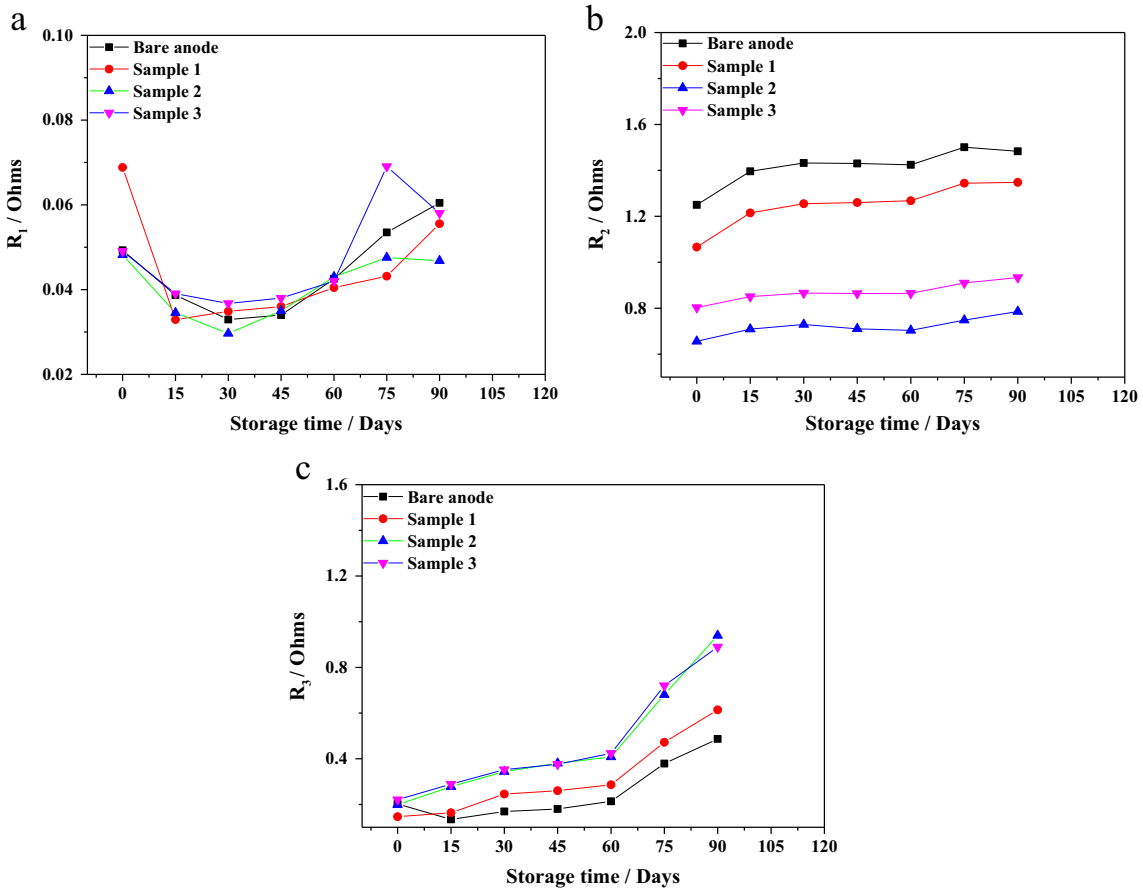

Fig. 11 Changes of the electrolyte resistance (**a**), the interphase resistance (**b**), and charge-transfer resistance (**c**) during storage at 55 °C. For each kind of anode, the values were obtained from the same cell during storage aging

involved in the Li^+ transportation, but had little impacts on the capacity during the lithiation/delithiation progress.

Figure 7 depicts the rate performance of $LiNi_{0.8}Co_{0.15}Al_{0.05}O_2$/graphite full cell with and without LiPON layer on anode. As can be seen in Fig. 7, the LiPON layer on anode did not have remarkable impacts on the capacity of the full cell at C/5, C/2, and 1C. However, when discharging at a higher rate (2C and 5C), the capacity was decreased along with the thickness of the LiPON layer on anode. The capacity retention was 80.8, 79.9, 79.4, and 76.5% at 2C and 47.7, 42.1, 36.4, and 28.0% at 5C, respectively, for bare anode, sample 1, sample 2, and sample 3 anodes.

Figure 8a–c shows the charge-discharge curves of the $LiNi_{0.8}Co_{0.15}Al_{0.05}O_2$/graphite full cell storage aged at 55 °C for different days, using anode with different thicknesses of LiPON. As seen in Fig. 8, there is no significant change on the discharge capacity of the cell with or without LiPON layer on anode before storage aging, which indicated that the LiPON layer did not affect the lithiation/delithiation of graphite anode at current charge-discharge rate (C/5) in full cell. However, an obvious improvement on the storage aging stability was observed upon storage aging at elevated temperature (55 °C). All the cells suffered capacity fading upon storage at elevated temperature. The discharge capacity of cell storage aged for 30 days were 188, 189, 187, and 185 mAh, respectively, for the bare anode, sample 1, sample 2, and sample 3 anodes. After storage aged for 90 days at 55 °C, the discharge capacity of cell with bare anode was 160 mAh or 80% capacity retention. However, the cells with sample 1 ~ 3 anode showed improved storage aging stability, 166, 174, 176 mAh (83, 87, and 88% capacity retention), respectively. Meanwhile, the storage aging results showed that the thicker LiPON layer on anode exhibited better capacity retention during storage aging.

The EIS of the cells during storage aging, along with the surface analysis of anode extract from anode with and without LiPON layer, as described below, provided insight into the sources of differences in capacity retention at elevated temperature.

The EIS analysis with and without LiPON

EIS simulation was a powerful tool to interpret the Li-ion and electron migration mechanism, interfacial phenomenon, and failure mechanisms [27, 28]. Figure 9 shows a typical impedance spectrum of the test full cell with or without LiPON layer on anode and a widely used equivalent circuit, representing both electrodes, the electrolyte and the current collectors [28]. In relation to the electrochemical processes, the resistance R_1, represented the resistance due to the electrolyte, was given by the intercept of impedance curves with the real axis in the Nyquist diagram. The semicircle, appearing at high frequency, represented the solid-electrolyte interphase resistance of both electrodes, while the smaller one, appearing at low frequency, represented the charge-transfer resistance. The R_2CPE_1-elements and R_3CPE_2-elements in the equivalent circuit represented the semicircle at high and low frequency, respectively. The Warburg element Wo represented the charge diffusion in the electrodes [28–30]. The elements in EIS of full cell, like

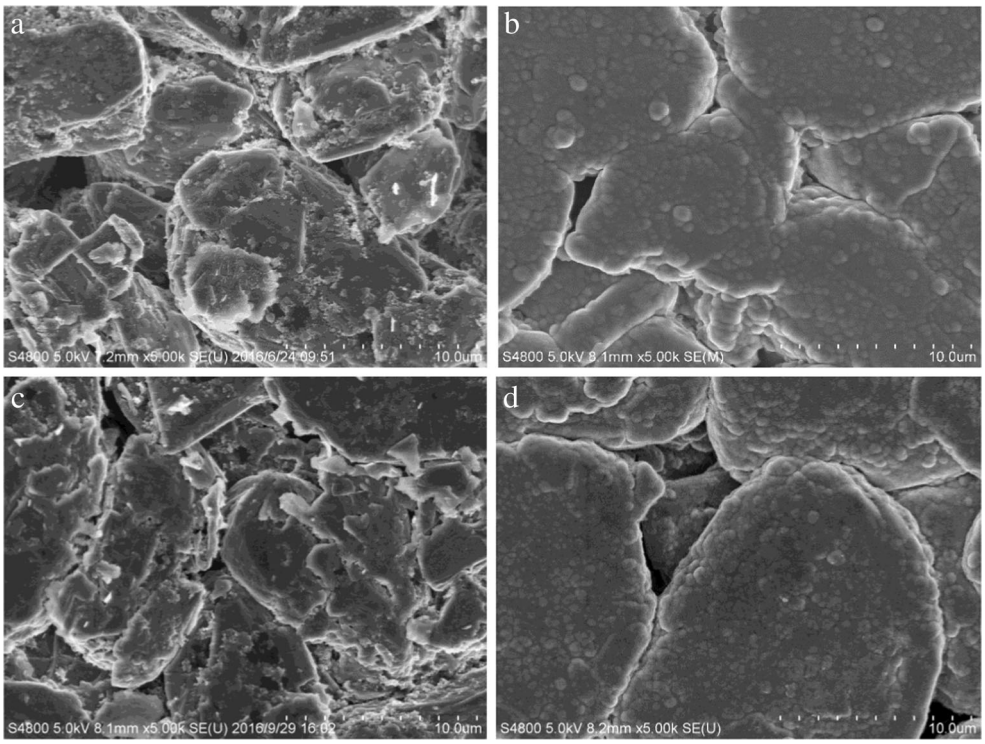

Fig. 12 The SEM micrograph of anode extracted from cell with **a** bare anode and **b** sample 2 anode before storage, and **c** bare anode and **d** sample 2 anode after storage aging at 55 °C for 90 days

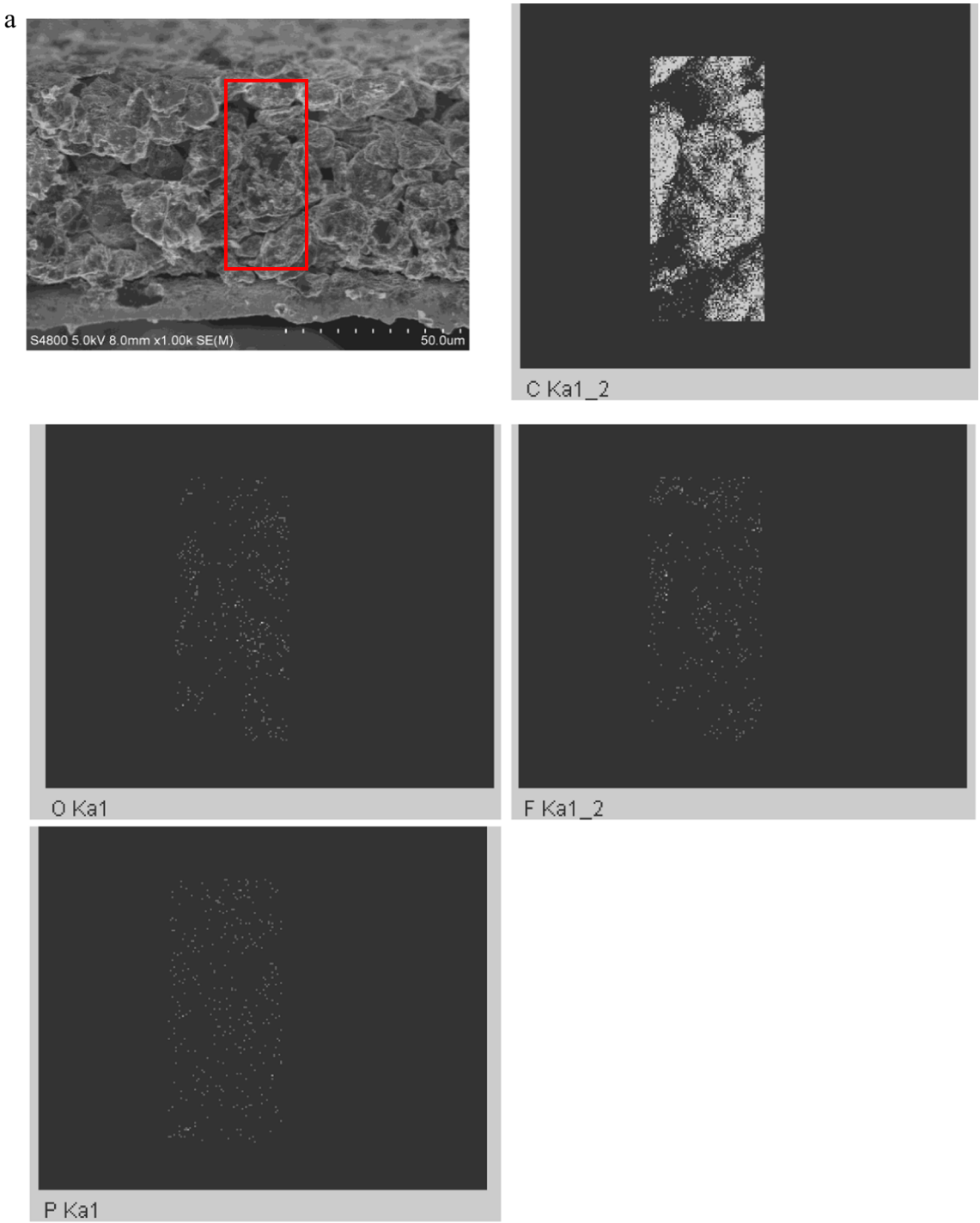

Fig. 13 The SEM side view of bare anode (**a**) and sample 2 anode (**b**) after storage aging at 55 °C for 90 days and its corresponding EDX elemental mapping

solid electrolyte resistance and charge-transfer resistance, were affected by both electrodes. Since the LiPON layer was only deposited on anode and would not have impacts on cathode, we could attribute the changes of full cell EIS to the impacts of LiPON layer on anode.

During storage aging, for every 15 days, the cells for EIS test were sampled and cooled, and then the EIS spectroscopy was recorded at room temperature, as shown in Fig. 10. The values of elements R_1, R_2, and R_3, which represented the electrolyte resistance, interphase resistance and charge-transfer resistance, respectively, were simulated by Zview. In Fig. 11, the simulated values of R_1, R_2, and R_3 during storage aging with different anodes were illustrated.

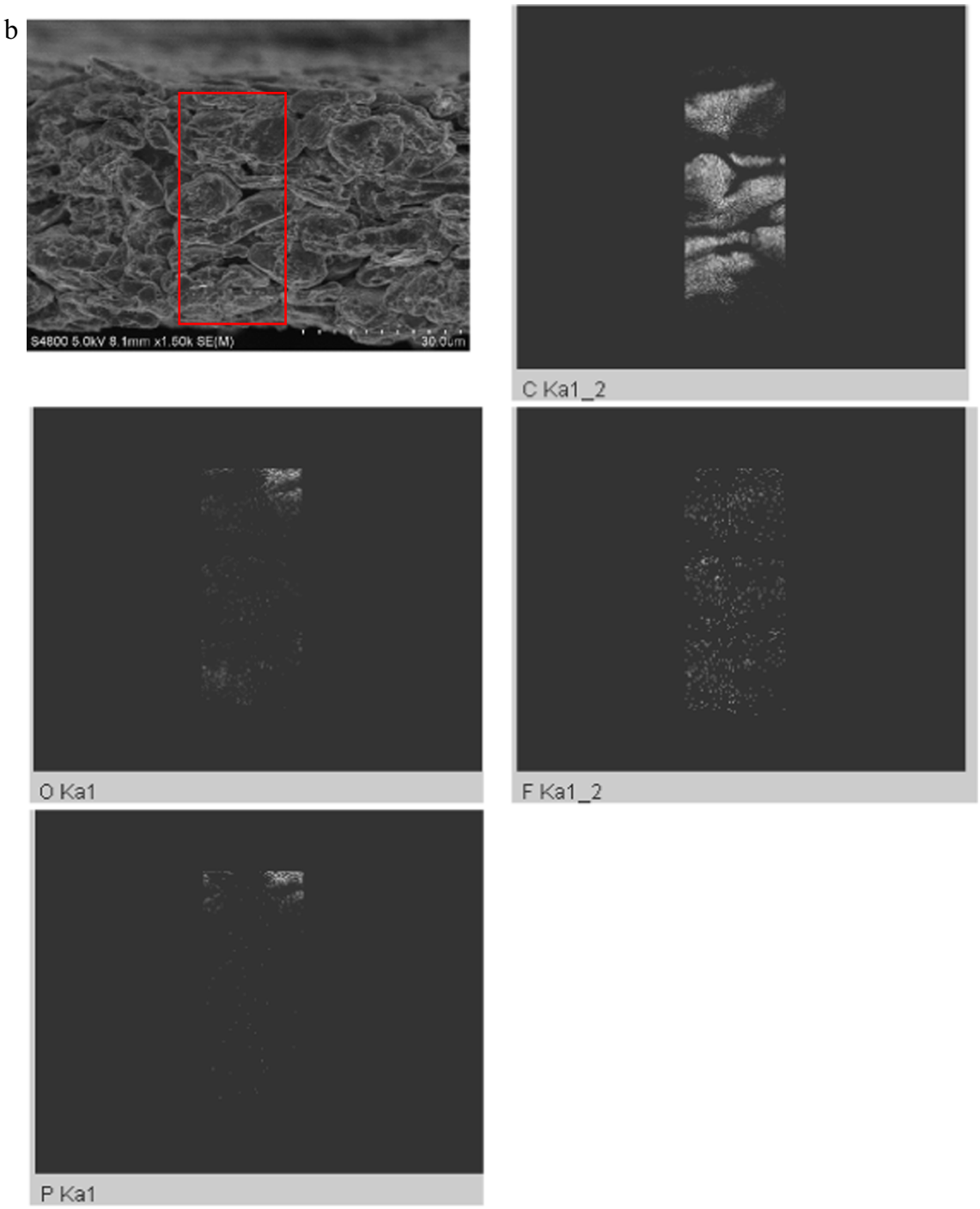

Fig. 13 (continued)

As can be seen in Fig. 11a, the LiPON layer on anode did not have much impact on the bulk resistance of the test cell before and during storage aging. Meanwhile, the simulated value of R_1 was much smaller than the values of R_2 and R_3 and the bulk resistance had only few changes during storage aging which may result from the test error and simulating error. It indicated that the ionic transportation of remaining electrolyte and LiPON layer was not remarkably affected during storage aging, though part of the electrolyte would be consumed.

However, the interphase resistance R_2 significantly decreased before storage and the increase of the interphase resistance R_2 during storage aging was restrained when the LiPON layer was sputtered on anode, as Fig. 11b shows. That might result from the resistance of the well-formed and attached anode-LiPON interphase would be smaller than the normal anode-electrolyte interphase resistance since the LiPON layer would act as electrolyte and R_2 was representing combination of the solid-electrolyte resistance. Meanwhile, the charge-transfer resistance R_3 became

larger and increased faster during aging with the addition of LiPON layer. The cell with the thickest LiPON layer exhibited the highest charge-transfer resistance, along with the highest capacity retention, as Fig. 11c shows. Since the full cell resistance, including interphase resistance and charge-transfer resistance, is the combination of the resistance of both electrodes [28, 30, 31], we could propose that the LiPON layer on anode decreased the anode/electrolyte interphase resistance and increased the charge-transfer resistance of the anode. The charge-transfer resistance could be used as a kinetic parameter to analyze the rate of faradic reaction while high charge-transfer resistance generally corresponded to low reaction rate [29]. Hence, the storage aging, mainly induced by the Li loss in anode which was caused by the corrosion of electrolyte [3, 4, 32], would be restrained by the increase of the charge-transfer resistance though the addition of LiPON layer on anode.

The improved capacity retention and increased charge-transfer resistance indicated that the LiPON layer would decrease the electrolyte corrosion rate with lithium in anode during storage aging. Based on our observation, we proposed an explanation for the effect. First, the LiPON layer on the top of the anode would protect the top of the graphite from electrolyte corrosion. Meanwhile, parts of the gap between graphite particles on the top of the anode would be blocked or narrowed during the sputtering process, resulting in longer electrolyte exchange routing from the inner part of the anode to the surface and ending in lower electrolyte corrosion rate on the surface the inner anode graphite during storage aging.

The SEM analysis of anode

To characterize the anode surface morphology after aging, cells were disassembled in Ar-filled glove box and a slice of anode was cut and cleaned by rinsing with pure DMC. Then, the slice of anode was transformed to the SEM chamber with exposure to air for about 30 s unfortunately. Fig. 12 shows the top view of the surface morphology of aged bare anode and sputtered anode (sample 2) before and after storage aging at 55 °C for 90 days. As shown in Fig. 12c, a rough layer was immersed on the graphite bare anode, compared with the fresh bare anode as shown in Fig. 12a, which resulted to the SEI growing on anode, induced by the decomposition of electrolyte [3, 8, 33]. However, there is no significant change on the surface morphology of the LiPON-protected aged anode, confirming that the LiPON layer would act as a protective layer and shut down the electrolyte corrosion on the top of anode.

Meanwhile, the side view of the aged anode was observed to analyze the inner part of the graphite in anode. Figure 13 shows the typical side view and its corresponding energy-dispersive X-ray spectroscopy (EDX) elemental mapping images of anode after storage aging at 55 °C for 90 days with and without LiPON layer on anode. As seen from the EDX mapping images, on the aged anode without LiPON, the elements, inluding oxygen (O), fluorine (F), and phosphorus (P), were evenly disctributed on the graphite particles from the surface to the bottom of the anode. However, on the aged anode with LiPON layer protected, the compcact distribution of P and O at the top of the anode was atributed to the LiPON layer. While the distribution of P and O in the inner part of the anode was more dispersive than the aged bare anode, the F distributuion was proportionate. The elements F, P, and O were originated from the following reactions (EC as an example for the electrolyte solvent) [34, 35]:

$$2EC + 2Li^+ + 2e^- \rightarrow (CH_2OCO_2Li)_2\downarrow + CH_2 = CH_2 \quad (1)$$

$$EC + 2Li^+ + 2e^- \rightarrow Li_2CO_3\downarrow + CH_2 = CH_2 \quad (2)$$

$$LiPF_6 \rightleftarrows LiF\downarrow + PF_5 \quad (3)$$

$$PF_5 + Li_2CO_3 \rightarrow LiPF_4O\downarrow + CO_2 + LiF\downarrow \quad (4)$$

that indicated the LiPON layer inhibited the decomposition of electrolyte solvent in the inner part of the anode since the elements of P and O was origin from the decomposition of the electrolyte solvents. That reconfirned the expalantion that the LiPON layer blocked or narrowed the gap between the graphite particles and inhibited the electrolyte exchange from the inner anode to the surface, resulting in lower rate of the electrolyte solvent corrosion in the anode, while the transportation of $LiPF_6$ (Li^+ and PF_6^- in electrolyte) was not affected since the transportation of ion (Li^+ and PF_6^-) was much easier than a molecule (electrolyte solvents) from the inner anode to the surface.

Conclusion

In this paper, we discussed the ability of LiPON layer-covered graphite anode, to significantly improve the capacity retention of pouch cells with $LiNi_{0.8}Co_{0.15}Al_{0.05}O_2$ cathode during storage aging. Three different thicknesses of LiPON layer on anode were prepared, and the capacity retention of cells during storage aging increased along with the growing of LiPON layer thickness. The thickest LiPON layer, about 1250 nm, exhibited 88% capacity retention at 55 °C for 90 days, compared with 80% for bare anode. The EIS analysis of cells with and without LiPON layer on anode revealed the cells with LiPON layer on anode would have smaller interphase resistance but larger charge-transfer resistance than cells with bare anode during storage aging, while these changes of impedances resulted in lower electrolyte corrosion rate and ended in higher capacity retention. The SEM micrograph confirmed the protective effect of LiPON layer as no significant corrosion products were observed on aged LiPON-covered anode, while on aged bare anode, significant SEI growing was observed. The EDX elemental mapping of the side view of the anode reconfirmed the corrosion of electrolyte solvent in

the inner part of the anode was restrained with the LiPON layer on the top of the anode.

Acknowledgements This work was supported by the Research Project of National University of Defense Technology (ZDYYJCYJ 20140701). Meanwhile, we would gratefully like to thank the Zhong Fang Gai De Vacuum Technology Co. Ltd., Beijing, China, for providing us the rf magnetron sputtering equipment.

References

1. Thomas EV, Bloom I, Christophersen JP, Battaglia VS (2012) Ratebased degradation modeling of lithium-ion cells. J Power Sources 206:378–382
2. Christophersen JP, Bloom I, Thomas E, Battaglia V (2012) Battery calendar life estimate manual modeling and simulation. INL/EXT-08015136
3. Agubra V, Fergus J (2013) Lithium ion battery anode aging mechanisms. Materials 6:1310–1325
4. Barré A, Deguilhem B, Grolleau S, Gérard M, Suard F, Riu D (2013) A review on lithium-ion battery ageing mechanisms and estimations for automotive applications. J Power Sources 241:680–689
5. Sarre G, Blanchard P, Broussely M (2004) Aging of lithium-ion batteries. J Power Sources 127:65–71
6. Schlasza C, Ostertag P, Chrenko D, Kriesten R (2014) Review on the aging mechanisms in Li-ion batteries for electric vehicles based on the FMEA method. Transportation Electrification Conference and Expo 1-6
7. Vetter J, Novák P, Wagner MR, Veit C, Möller KC, Besenhard JO, Winter M, Wohlfahrt-Mehrens M, Vogler C, Hammouche A (2005) Ageing mechanisms in lithium-ion batteries. J Power Sources 147: 269–281
8. Waldmann T, Wilka M, Kasper M, Fleischhammer M, Wohlfahrt-Mehrens M (2014) Temperature dependent ageing mechanisms in Lithium-ion batteries – a post-mortem study. J Power Sources 262: 129–135
9. Broussely M, Herreyre S, Biensan P, Kasztejna P, Nechev K, Staniewicz RJ (2001) Aging mechanism in Li ion cells and calendar life predictions. J Power Sources 97-98:13–21
10. Roberts M, Biendicho JJ, Hull S, Beran P, Gustafsson T, Svensson G, Edström K (2013) Design of a new lithium ion battery test cell for in-situ neutron diffraction measurements. J Power Sources 226:249–255
11. Prasad GK, Rahn CD (2013) Model based identification of aging parameters in lithium ion batteries. J Power Sources 232:79–85
12. Yoshida T, Takahashi M, Morikawa S, Ihara C, Katsukawa H, Shiratsuchi T, Yamaki JI (2006) Degradation mechanism and life prediction of lithium-ion batteries. J Jpn Soc Nat Disaster Sci 153: A576–A582
13. Xu K (2014) Electrolytes and interphases in li-ion batteries and beyond. Chem Rev 114:11503
14. Verma P, Maire P, Novák P (2010) A review of the features and analyses of the solid electrolyte interphase in Li-ion batteries. Electrochim Acta 55:6332–6341
15. An SJ, Li J, Danie C, Mohanty D, Nagpure S, Wood DL (2016) The state of understanding of the lithium-ion-battery graphite solid electrolyte interphase(SEI) and its relationship to formation cycling. Carbon 105:52–76
16. Li NW, Yin YX, Yang CP, Guo YG (2016) An artificial solid electrolyte interphase layer for stable lithium metal anodes. Adv Mater 28:1853
17. Li J, Dudney NJ, Nanda J, Liang C (2014) Artificial solid electrolyte interphase to address the electrochemical degradation of silicon electrodes. Acs Appl Mater Int 6:10083–10088
18. Lin YX, Liu Z, Leung K, Chen LQ, Lu P, Qi Y (2016) Connecting the irreversible capacity loss in Li-ion batteries with the electronic insulating properties of solid electrolyte interphase (SEI) components. J Power Sources 309:221–230
19. Wu NL, Weng YT, Li FS, Yang NH, Kuo CL, Li DS (2015) Polymeric artificial solid/electrolyte interphases for Li-ion batteries. Prog Nat Sci Mater Int 25:563–571
20. Van-Jodin LL, Ducroquet F, Sabary F, Chevalier I (2013) Dielectric properties, conductivity and Li+ ion motion in LiPON thin films. Solid State Ionics 253:151–156
21. Senevirathne K, Day CS, Gross MD, Lachgar A, Holzwarth NW (2013) A new crystalline LiPON electrolyte: synthesis, properties, and electronic structure. Solid State Ionics 233:95–101
22. Dudney NJ (2000) Addition of a thin-film inorganic solid electrolyte (Lipon) as a protective film in lithium batteries with a liquid electrolyte. J Power Sources 89:176–179
23. Jouybari YH, Berkemeier F (2016) Enhancing silicon performance via LiPON coating: a prospective anode for lithium ion batteries. Electrochim Acta 217:171–180
24. Kim Y, Veith GM, Nanda J, Unocic R, Chi M, Dudney NJ (2011) High voltage stability of LiCoO2 particles with a nano-scale Lipon coating. Electrochim Acta 56:6573–6580
25. Nimisha CS, Rao KY, Venkatesh G, Rao GM, Munichandraiah N (2011) Sputter deposited LiPON thin films from powder target as electrolyte for thin film battery applications. Thin Solid Films 519: 3401–3406
26. Bridges CA, Sun XG, Zhao J, Paranthaman MP, Dai S (2012) In situ observation of solid electrolyte interphase formation in ordered mesoporous hard carbon by small-angle neutron scattering. J Phys Chem C 116:7701–7711
27. Liu L, Park J, Lin X, Sastry AM, Lu W (2014) A thermalelectrochemical model that gives spatial-dependent growth of solid electrolyte interphase in a Li-ion battery. J Power Sources 268:482–490
28. Reichert MDA, Rösmann A, Janssen P, Bremes HG, Sauer DU, Passerini S, Winter M (2013) Influence of relaxation time on the lifetime of commercail lithium-ion cells. J Power Sources 239:45–53
29. Zhang SS, Xu K, Jow TR (2004) Electrochemical impedance study on the low temperature of Li-ion batteries. Electrochim Acta 49: 1057–1061
30. Prada E, Domenico DD, Creff Y, Bernard J, Sauvant-Moynot V, Huet F (2013) A simplified electrochemical and thermal aging model of LiFePO4-graphite Li-ion batteries: power and capacity fade simulations. J Electrochem Soc 160:A616–A628
31. Zhang D, Haran BS, Durairajan A, White RE, Podrazhansky Y, Popov BN (2000) Studies on capacity fade of lithium-ion batteries. J Power Sources 91:122–129
32. Bodenes L, Naturel R, Martinez H, Dedryvère R, Menetrier M, Croguennec L, Pérès JP, Tessier C, Fischer F (2013) Lithium secondary batteries working at very high temperature: capacity fade and understanding of aging mechanisms. J Power Sources 236: 265–275
33. Röder P, Stiaszny B, Ziegler JC, Baba N, Lagaly P, Wiemhöfer HD (2014) The impact of calendar aging on the thermal stability of a LiMn2O4– Li(Ni1/3Mn1/3Co1/3)O2/graphite lithium-ion cell. J Power Sources 268:315–325
34. Agubra VA, Fergus JW (2014) The formation and stability of the solid electrolyte interface on the graphite anode. J Power Sources 268:153–162
35. Xu K, Lee U, Zhang SS, Jow TR (2004) Graphite/electrolyte interface formed in LiBOB-based electrolytes, II potential dependence of surface chemistry on graphitic anodes. J Electrochem Soc 151: A2106–A2112